Global Energy Interconnection 8 (2025) 420–432

KeAi
CHINESE ROOTS
GLOBAL IMPACT

Global Energy Interconnection
Development and Cooperation Organization

Global Energy Interconnection

Contents lists available at ScienceDirect
journal homepage: www.elsevier.com/locate/gloei

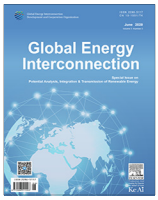

Online evaluation method for MMC submodule capacitor aging based on CapAgingNet

Xinlan Deng [a,b], Youhan Deng [a,c], Liang Qin [a,b,*], Weiwei Yao [a,c], Min He [a,b], Kaipei Liu [a,b]

[a] *Laboratory of Hydro-Wind-Solar Multi-energy Control Coordination, Wuhan 430000, P.R. China*
[b] *School of Electrical and Automation, Wuhan University, Wuhan 430072, P.R. China*
[c] *Institute of Science and Technology, China Three Gorges Corporation, Beijing 101100, P.R. China*

Received 30 July 2024; revised 5 March 2025; accepted 17 March 2025

Abstract

Submodule capacitor aging poses significant challenges to the safe operation of modular multilevel converter (MMC) systems. Traditional detection methods rely predominantly on offline tests, lacking real-time evaluation capabilities. Moreover, existing online approaches require additional sampling channels, thereby increasing system complexity and costs. To address these issues, this paper proposes an online evaluation method for submodule capacitor aging based on CapAgingNet. Initially, an MMC system simulation platform is developed to examine the effects of submodule capacitor aging on system operational characteristics and to create a dataset of submodule capacitor switching states. Subsequently, the CapAgingNet model is introduced, incorporating key technical modules to enhance performance: the Deep Stem module, which extracts larger receptive fields through multiple convolution layers and mitigates the impact of data sparsity in capacitor aging on feature extraction; the efficient channel attention (ECA) module, utilizing one-dimensional convolution for dynamic weighting to adjust the importance of each channel, thereby enhancing the ability of the model to process high-dimensional features in capacitor aging data; and the multiscale feature fusion (MSF) module, which integrates capacitor aging information across different scales by combining fine-grained and coarse-grained features, thus improving the capacity of the model to capture high-frequency variation characteristics. The experimental results reveal that the CapAgingNet model achieves a TOP-1 accuracy of 95.32 % and a macro-averaged F_1 score of 95.49 % on the test set, thereby providing effective technical support for online monitoring of submodule capacitor aging.

Keywords: Modular multilevel converter; Capacitor aging; Condition monitoring; Fault diagnosis

0 Introduction

As the proportion of new energy generation grows, traditional AC power grids face significant challenges due to large-scale, highly variable, and unpredictable energy sources. Flexible DC grids, utilizing voltage source converters and bidirectional controllable power electronic devices, excel in integrating renewable energy. Among these, the modular multilevel converter (MMC) stands out for its low harmonic distortion, minimal switching losses, and high modularity, contributing to its extensive adoption in flexible DC transmission systems [1,2].

MMC achieves efficient energy conversion and precise voltage control by assembling numerous submodules to create multilevel outputs. Submodule capacitors are crucial components of MMC converter valves and are essential for voltage balancing, energy storage, and harmonic filtering. Metallized polypropylene film capacitors (MPPF)

* Corresponding author at: Laboratory of Hydro-Wind-Solar Multi-energy Control Coordination, Wuhan 430000, China.
E-mail addresses: 2018302070241@whu.edu.cn (X. Deng), yhdeng@whu.edu.cn (Y. Deng), qinliang@whu.edu.cn (L. Qin), yao_weiwei@ctg.com.cn (W. Yao), whuhemin@whu.edu.cn (M. He), kpliu@whu.edu.cn (K. Liu).

https://doi.org/10.1016/j.gloei.2025.03.002

are predominantly employed in MMCs owing to their compact size, low inductance, and excellent self-healing capabilities [3]. However, during prolonged operation, submodule capacitors endure thermal, electrical, and mechanical stresses, leading to aging. This aging process can decrease capacitance and increase equivalent series resistance, thereby escalating losses and temperatures, deteriorating the operating conditions of the device, and initiating a vicious cycle [4]. Therefore, accurately detecting the aging degree of MMC metallized film capacitors is essential for maintaining the performance and reliability of the equipment.

Methods for monitoring submodule capacitor aging can be divided into offline detection and online monitoring techniques based on whether the converter needs to be shut down. Offline detection involves proactively shutting down the converter during routine maintenance to evaluate the capacitors, using LCR bridges to precisely measure parameters like capacitance and equivalent series resistance [5]. Although this method does not account for the operational characteristics of the converter, it is unsuitable for applications requiring continuous operation. Moreover, it becomes impractical for systems with numerous capacitors or complex converter structures owing to high costs and operational challenges.

Conversely, online monitoring allows real-time tracking of capacitor status without interrupting converter operation, making it an ideal choice for condition monitoring. Regarding online monitoring of MMC submodule capacitor aging, several approaches have been explored:

In [6], a controlled AC signal at twice the fundamental frequency was injected into the MMC circulating current loop to produce current and voltage ripples in the submodule capacitors, facilitating the calculation of their values. However, this method increased system losses and required additional power supply installations. [7] determined submodule capacitor values by analyzing the inherent second harmonics in the submodule capacitor voltage and current. [8] proposes a fault detection and fault-tolerant scheme for MMC-HVDC systems based on a sliding mode observer, which predicts the submodule voltage by establishing a sliding mode observer on the submodule voltage. [9] actively discharges submodule capacitors using parallel discharge resistors and determines capacitor values based on discharge time.

However, voltage fluctuations from active discharging can impact the MMC's output performance. Another study [10] investigates aluminum electrolytic capacitors and introduces an online capacitor value estimation method using recursive least squares. [11] streamlines the calculation by selecting the submodule with the largest capacitance as a reference and assessing the relative capacitance of other submodules. [12] monitors capacitor aging in real-time by measuring the relative values of submodule capacitors, leveraging the correlation between voltage changes and capacitance values. [13] determines capacitor aging status by analyzing the high-frequency band energy of the output voltage. [14] proposes a remaining life estimation strategy for metallized polypropylene film capacitors based on the interplay among ESR, capacitance aging rate, and temperature. [15] presents a method combining wavelet transform and CNN to estimate capacitor parameters by extracting low- and mid-frequency features from the capacitor voltage.

In summary, current methods for monitoring the aging of metallized polypropylene film capacitors have several limitations: offline approaches are complex, time-consuming, and offer only static information. Although online detection methods improve detection efficiency, they require the measurement of submodule capacitor current, making the monitoring process more complex. Moreover, the need for additional sampling channels elevates system costs, whereas enhancing detection accuracy and speed remains imperative.

Recently, artificial intelligence has been extensively adopted within power systems. Specifically, for capacitor aging monitoring, aging can be automatically identified by tracking capacitors' voltage, current, and switching states, thereby improving the efficiency and precision of aging assessments. Building upon the analysis of MMC aging characteristics, this study employs submodule switching state data for monitoring purposes. This data represents discrete time-series signals marked by sparsity and multi-timescale fluctuations. Additionally, neural networks extract high-dimensional semantic features from these signals. The data encompass rich temporal information and intricate features, illustrating complex behaviors of capacitors across various aging stages. Sparse data require the model to effectively capture and utilize key features; high-dimensional features increase the complexity of data processing and classification; and multi-timescale variations hinder the model from accurately detecting changes across different time scales.

To address the challenges in capacitor aging monitoring using artificial intelligence methods, such as insufficient feature extraction from sparse data, inadequate processing of high-dimensional features, and the absence of multiscale features, this study proposes the CapAgingNet algorithm, which integrates three improved modules:

1) Deep Stem Module: This module gradually expands the receptive field to enhance the diversity and granularity of feature extraction, addressing the issue of insufficient low-level feature extraction from sparse data.
2) ECA Module: This module modulates channel weights via adaptive dynamic 1D convolution, thereby enhancing the representation of critical features and increasing the model's ability to capture high-dimensional features.

3) MSF Module: This module consolidates feature information across multiple levels, thereby improving the accuracy and robustness of feature extraction and resolving the issue of missing multiscale features.

The experimental results indicate that CapAgingNet outperforms in capacitor aging detection tasks, effectively identifying subtle changes in capacitor switching states and accurately assessing capacitor aging status. This provides robust technical support for the condition monitoring and lifetime evaluation of submodule capacitors in MMC.

1 Principle of MMC operation and capacitor aging analysis

1.1 Principle of MMC operation

The three-phase MMC topology is depicted in Fig. 1. Each converter consists of six arms, with each arm comprising multiple cascaded submodules connected in series. Each arm includes an arm inductor, L_0, and N identical submodules. The upper and lower arms of the same phase form a phase unit. The half-bridge submodule is the most commonly used type, comprising two IGBTs with anti-parallel diodes connected in series and a capacitor connected in parallel. V_{T1} and V_{T2} represent the IGBTs, V_{D1} and V_{D2} denote the anti-parallel diodes connected across the IGBTs, and C_0 indicates a DC-side energy storage capacitor. u_c denotes the voltage of the submodule DC-side energy storage capacitor, u_{sm} represents the output voltage at the submodule port, and i_{sm} denotes the current flowing into the submodule. The DC-side energy storage capacitor within the submodule maintains the DC voltage.

MMC utilizes a nearest level modulation strategy, generating a staircase waveform that approximates a sinusoidal waveform on the AC side by producing multiple voltage levels. Each staircase voltage level closely corresponds to the submodule operations and is approximately equal to the voltage of a submodule capacitor. For example, in a half-bridge MMC submodule, toggling the IGBTs on and off effectively inserts or removes the submodule, as illustrated in Fig. 2.

1.2 Aging mechanism of metallized polypropylene film capacitors

Metallized polypropylene film capacitors are typically fabricated from polypropylene using winding and metal spraying techniques. The primary aging factors include self-healing dielectric breakdown, electrode area reduction due to metal oxidation, and dielectric film failure [16]. Although metallized film capacitors possess self-healing capabilities, this process gradually leads to aging and eventual failure, as shown in Fig. 3. During manufacturing, defects known as electrical weak points may form on the film due to process imperfections. These weak points have lower breakdown field strength compared to the surrounding areas. During capacitor operation, these electrical weak points are the first to undergo breakdown, creating discharge channels. The discharge results in a rapid temperature increase, causing the metal layer to evaporate and ionize. As the discharge arc extinguishes, the electrical weak point is removed and an insulation halo is formed, thereby completing the self-healing process [17]. Through-

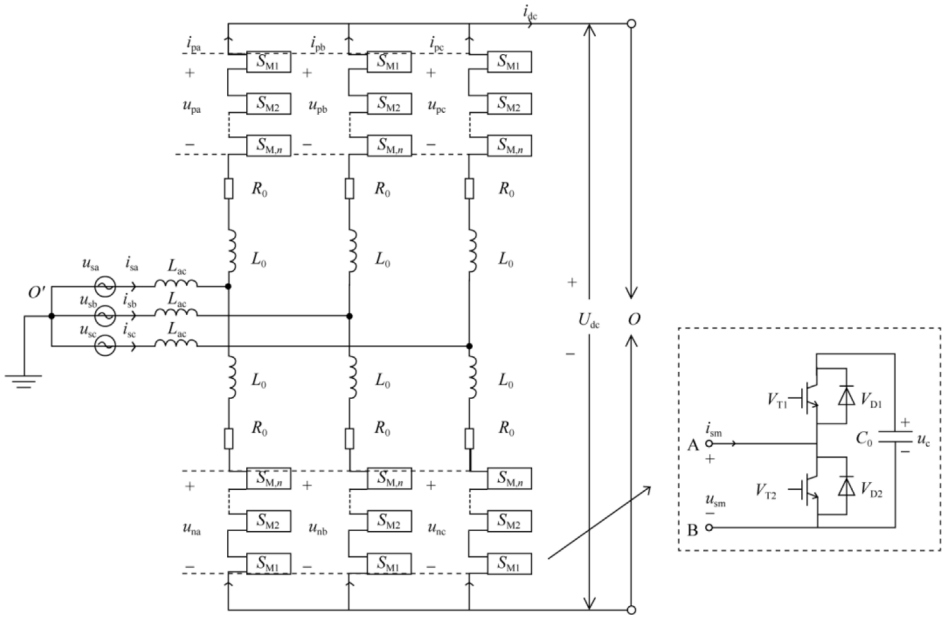

Fig. 1. Topology of a three-phase MMC and a single half-bridge submodule.

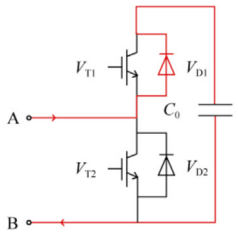

(a) V_{T1} is on, V_{T2} is off, current flows from A to B, submodule is inserted

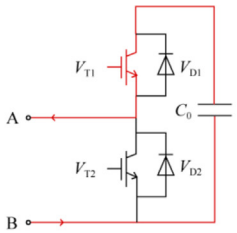

(b) V_{T1} is on, V_{T2} is off, current flows from B to A, submodule is inserted

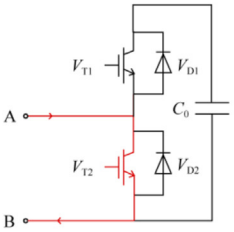

(c) V_{T1} is off, V_{T2} is on, current flows from A to B, submodule is bypassed

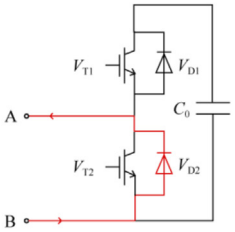

(d) V_{T1} is off, V_{T2} is on, current flows from B to submodule is bypassed

Fig. 2. Submodule working status.

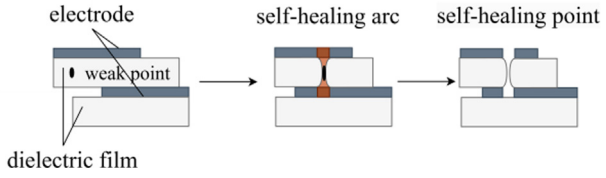

Fig. 3. Self-healing process of metal film capacitor.

out this process, the capacitor undergoes a slight reduction in capacitance. As the number of breakdown points increases, the capacitance of the metallized film capacitor progressively diminishes until failure ensues. In practical engineering applications, a metallized polypropylene film capacitor is deemed failed when its capacitance drops by more than 5 % [18].

1.3 Analysis of the correlation between capacitor aging and submodule switching states

According to the operational principles of MMC, the switching state of submodules relies on the number of submodules that need activation during the current control cycle, the direction of the arm current, and the sequence of capacitor voltages. As capacitance decreases, the charging and discharging rates of the capacitor escalate. With a constant charging current, the voltage variation becomes more pronounced. In MMC, all inserted submodule capacitors are connected in series, ensuring equal current flow. When a submodule capacitor experiences slight aging, the reduced capacitance accelerates the charging and discharging rates, resulting in more frequent submodule switching within each control cycle, thereby increasing the switching frequency. However, as the capacitor undergoes severe aging, its capacitance further declines, and its energy storage capability is substantially weakened. In this case, the capacitor cannot effectively store and release energy, and the voltage rapidly attains the cutoff threshold within a control cycle, which lowers the switching frequency.

Fig. 4 demonstrates the effect of capacitor aging on switching frequency.

Under normal operation, the submodule capacitor's voltage waveform aligns with the pattern shown in Fig. 4 (a). The submodule activates at t_0, remains active for three control cycles, and is then bypassed as its voltage rises from point A to B. At t_1, it is reactivated, conducts for another three control cycles, and is subsequently bypassed again, with the voltage increasing from B to C. Throughout this sequence, submodule 1 conducts twice, ensuring a stable switching frequency.

When submodule 1 experiences mild aging, its capacitance slightly decreases, accelerating its charging and discharging rates and causing larger voltage fluctuations. As illustrated in Fig. 4(b), after activation at t_0, its voltage increases from A to D within a single control cycle. At this stage, the voltage of the submodule 1 exceeds that of the other submodules, prompting an earlier bypass. Once the voltages of the other submodules exceed that of submodule 1, it is reinserted. During this period, as depicted in Fig. 4(b), submodule 1 conducts four times, resulting in a higher switching frequency compared to the normal state.

When submodule 1 experiences severe aging, its capacitance decreases significantly, which causes its voltage to increase drastically to C within a single control cycle and

immediately reach the cutoff threshold. Fig. 4(c) illustrates that submodule 1 is directly bypassed and operates only once during the process, resulting in a lower switching frequency compared to normal conditions.

To further validate this, a 21-level MMC system simulation platform was developed in MATLAB/Simulink, with system parameters specified in Table 1. The switching state of submodule 1 was selected as the monitoring variable, whereas the capacitance values of all other submodules were maintained at the designed 3 mF. Simulations were conducted by decrementing the capacitance of the submodule 1 by 1 % increments from its designed value, and the results are presented in Fig. 5.

The findings indicate that as the capacitors in certain MMC submodules age, their switching frequencies initially increase. However, when the capacitance decreases by more than 40 %, the switching frequency begins to decline. For metallized polypropylene film capacitors, a capacitance reduction exceeding 5 % is indicative of aging and failure. Therefore, during the transition from normal operation to aging failure of the metallized film capacitor, the

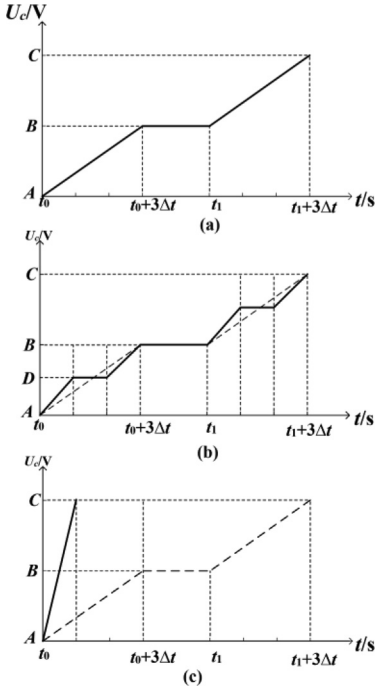

Fig. 4. Switching state of submodule 1 when the aging degree of capacitor is different.

Table 1
Parameters of MMC simulation model.

System Parameters	Values
DC side voltage	400 kV
Number of bridge arm submodules	20
Bridge inductance	15.92 mH
Submodule capacitance	3 mF
Base wave frequency	50 Hz

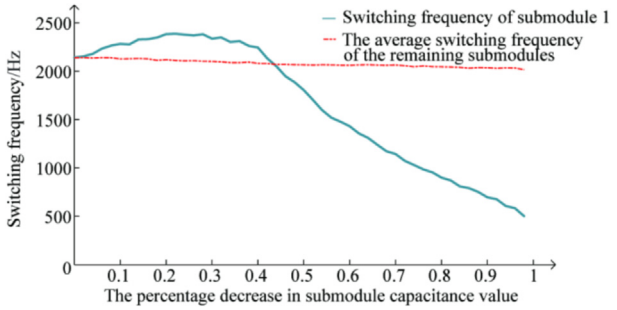

Fig. 5. Comparison of casting frequency between sub-module 1 and other sub-modules at different aging levels.

overall switching frequency of the submodule increases (see Fig. 6).

The increased switching frequency of severely aged submodules can cause the following hazards to the MMC:

1) The increased switching frequency leads to more frequent conduction of switching devices within the submodule, resulting in higher switching losses and a reduced lifespan of the switching devices.
2) Capacitor aging leads to increased heat generation within the capacitor, whereas higher switching frequencies further enhance heat dissipation in the switching devices. Consequently, this results in a rise in temperature that accelerates device aging, creating a vicious cycle.

Analyzing the relationship between submodule switching frequency and capacitor aging reveals that variations in switching states partially indicate the extent of capacitor aging. However, comprehensively understanding the aging state of submodules based solely on switching frequency changes is challenging. To address this, this study employs data analysis techniques to conduct an in-depth examination of submodule switching state data. By introducing classification models, extensive switching data are analyzed and categorized, thereby extracting valuable aging information from the large volume of complex data. This enables more accurate predictions of the aging state of submodules, thereby enhancing system maintenance efficiency and operational reliability.

2 Capacitor aging detection based on improved CapAgingNet

2.1 Principle of CSPResNeXt-50

CSPResNeXt-50 integrates the cross-stage partial network (CSPNet) and ResNeXt architectures to improve feature extraction capabilities and computational efficiency [19]. Its structure is illustrated in Fig. 5. The architecture includes an initial feature extraction stage using a Stem Layer with a 7 × 7 convolution kernel, four CSP

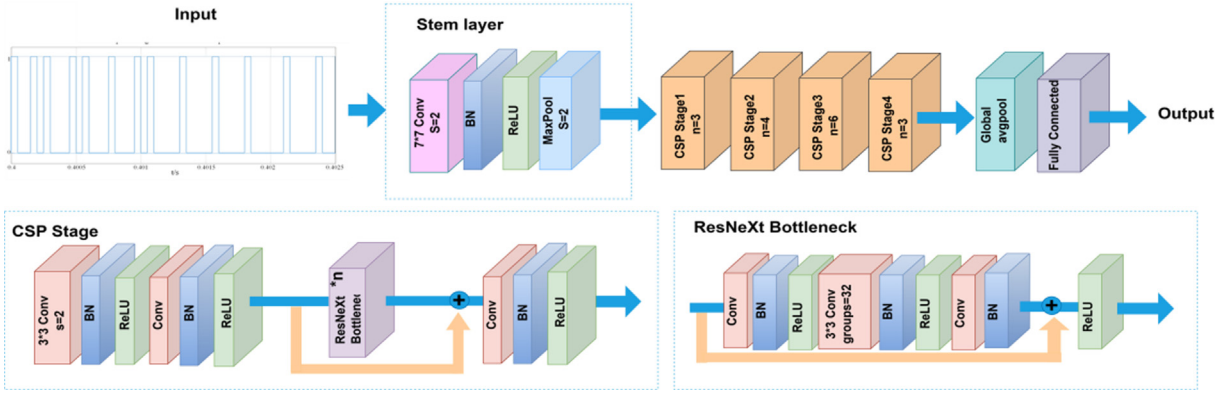

Fig. 6. Structure of the CSPResNeXt50 model.

stages composed of multiple ResNeXt Bottleneck modules to optimize gradient flow and computational efficiency, a global average pooling layer, and a fully connected layer for final classification.

CSPResNeXt-50 delivers potent feature extraction and computational efficiency. Deep convolutional networks can extract key features from high-frequency temporal signals, whereas the partial connections and cross-stage fusion of the CSPNet enhance gradient flow and promote effective learning during deep network training. This architecture adeptly captures the dynamic characteristics of signals, discerning time-series variations in capacitors across diverse aging states. It boosts the efficiency of feature extraction and classification tasks while minimizing computational resource usage, rendering it highly applicable for practical applications.

2.2 CapAgingNet model

To further advance the performance of CSPResNeXt-50, this study introduces CapAgingNet, which incorporates enhancements in three principal areas. The architecture of CapAgingNet is depicted in Fig. 7:

Enhanced Feature Extraction: The Deep Stem module incrementally broadens the receptive field, increasing the diversity and precision of feature extraction. This enables superior capturing of intricate behaviors under varying capacitor aging conditions.

Advanced High-Dimensional Feature Processing: The ECA module dynamically modulates each channel's importance using one-dimensional convolutional weighting, thereby augmenting the model's capability to process high-dimensional features in capacitor aging data.

Multiscale Feature Integration: The MSF module consolidates and interacts with features across multiple levels. By harnessing information from various feature scales, feature extraction accuracy is improved, facilitating more precise identification of capacitor aging states.

2.2.1 Deep stem module

In deep learning network architectures, the stem layer is pivotal for initial feature extraction. The standard CSPResNeXt-50 architecture utilizes a single 7×7 convolutional kernel for this function. In this work, the proposed Deep Stem module enhances feature extraction by replacing the lone 7×7 convolution with three consecutive 3×3 incremental dilated convolutions.

As depicted in Fig. 8, these incremental dilated convolutions successively increase the dilation rate, thereby enlarging the receptive field. A single 7×7 convolution

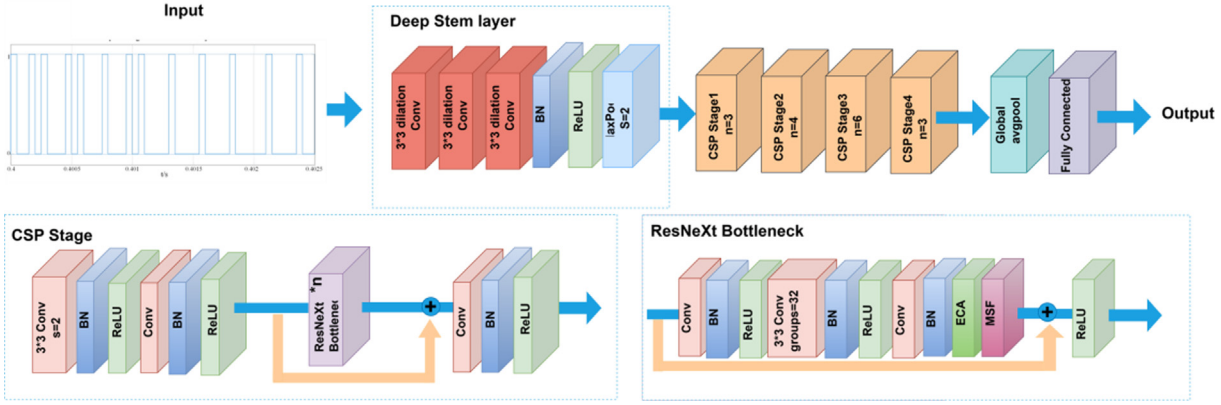

Fig. 7. Structure of the CapAgingNet model.

has a receptive field of 7 × 7, whereas three successive 3 × 3 incremental dilated convolutions achieve receptive fields of 3 × 3, 5 × 5, and 7 × 7, respectively. Consequently, the cumulative receptive field of the three incremental dilated convolutions exceeds that of a single 7 × 7 convolution. Gradually increasing the dilation rate enables a smooth expansion of the receptive field, allowing for the incorporation of more contextual information while maintaining the effectiveness of the convolution operations.

The number of parameters and computational complexity of a single 7 × 7 convolution are detailed in Eqs. (1) and (2):

$$\text{Parameter Count} = 7 \times 7 \times C_{\text{in}} \times C_{\text{out}} \tag{1}$$

C_{in} and C_{out} denote the input and output channel numbers, respectively.

$$\text{Computational Complexity} = 7 \times 7 \times H \times W \times C_{\text{in}} \times C_{\text{out}} \tag{2}$$

H and W represent the height and width of the input feature map, respectively.

For three consecutive 3 × 3 incremental dilated convolutions, the total number of parameters and computational complexity are shown in Equations (3) and (4):

$$\text{Total Parameter Count} = 3 \times 3 \times 3 \times C_{\text{in}} \times C_{\text{mid}} \tag{3}$$

C_{mid} denotes the intermediate channel number.

$$\text{Computational Complexity} = 3 \times (3 \times 3 \times H \times W \times C_{\text{in}} \times C_{\text{mid}}) \tag{4}$$

Even when $C_{\text{mid}} = C_{\text{in}}$, the Deep Stem module boasts fewer parameters and lower computational complexity compared to a single 7 × 7 convolution.

By employing multiple consecutive incremental dilated convolutions, the Deep Stem module progressively expands the receptive field while maintaining computational efficiency. Unlike conventional large convolution kernels, incremental dilated convolutions smoothly encompass a larger receptive field, capturing more contextual information and enhancing feature extraction diversity. Convolution kernels with varying dilation rates extract features at multiple levels, making them particularly suitable for sparse data signals and enhancing the model's sensitivity and ability to capture sparse data. Consequently, this improves the richness and precision of feature representation. Additionally, the progressively increasing receptive field facilitates better gradient flow, mitigating gradient vanishing or exploding issues associated with large receptive fields and enhancing training stability. Therefore, the Deep Stem module outperforms traditional large convolution kernels in receptive field coverage, feature extraction, and computational efficiency, establishing it as a more effective initial feature extraction method.

2.2.2 ECA module

The ECA [20] module is a lightweight attention mechanism designed to enhance convolutional neural networks by efficiently allocating attention across the channel dimension, thereby improving the expression of significant features. The structure of the ECA module is illustrated in Fig. 9.

The ECA module enhances the performance of channel attention mechanisms through a series of efficient steps. First, an input feature map χ with dimensions $C \times H \times W$ is passed through a global average pooling layer to produce a one-dimensional channel descriptor of length C.

$$z_c = \frac{1}{H \times W} \sum_{i=1}^{H} \sum_{j=1}^{W} X_{c,i,j}, c = 1, 2, ..., C \tag{5}$$

This descriptor then undergoes a parameter-free 1D convolution with a kernel size k defined by $k = \psi(C)$, typically an odd number, to effectively capture local cross-channel dependencies.

$$k = \psi(C) = \left| \frac{\log_2(C)}{\gamma} + b \right|_{odd} \tag{6}$$

where γ and b denote adjustable parameters, and $|\dot{s}|_{\text{odd}}$ represents rounding up to the nearest odd number.

After the 1D convolution, the resulting vector is processed by a Sigmoid activation function, mapping the weight of each channel to the [0, 1] range and generating a channel weight vector that reflects the significance of each channel. This weight vector is subsequently applied to the original input feature map through channel-wise multiplication, thereby re-weighting the channels to amplify the responses of the most important ones and enhance the feature expression capability.

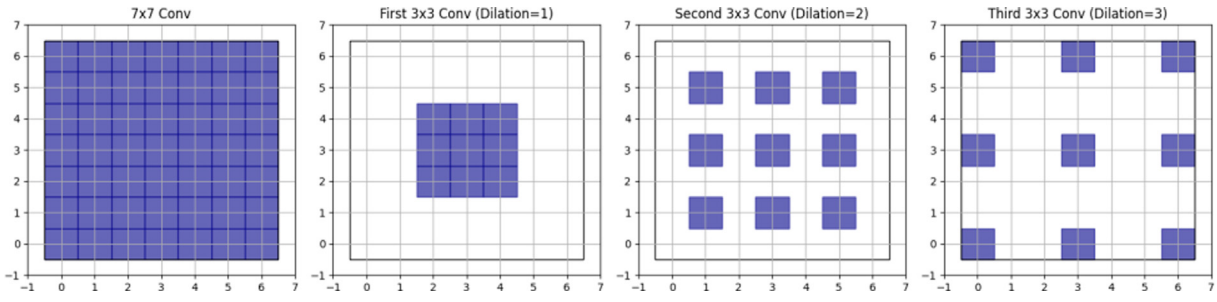

Fig. 8. Comparison of Receptive Field Sizes.

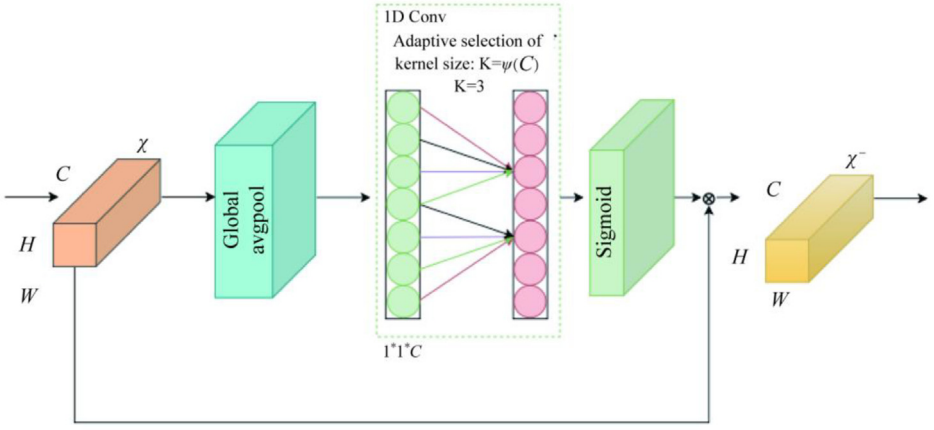

Fig. 9. ECA module structure.

The ECA module proficiently handles high-dimensional data, meticulously capturing subtle variations and intricate patterns in waveforms during capacitor aging. This effective processing allows the ECA module to establish precise dependencies between different feature channels, thereby more accurately identifying various stages of capacitor aging. By dynamically adjusting the importance of each channel, the ECA module becomes increasingly sensitive to minor fluctuations, resulting in a more accurate assessment of the aging state. Additionally, the ECA module can adapt to signal variations under different aging patterns and load conditions, enhancing the robustness and adaptability of the model in various application scenarios. These characteristics make the ECA module highly valuable for monitoring capacitor aging, significantly enhancing diagnostic accuracy and reliability.

2.2.3 MSF module

During convolutional neural network training, lower-layer features preserve high-resolution local details, enabling the detection of subtle changes in capacitor aging. Conversely, higher-layer features—extracted through multiple convolution and pooling operations—provide more abstract global information, effectively capturing long-term trend changes. The MSF module improves feature extraction accuracy by integrating information across various feature levels, leading to more precise identification of capacitor aging states. This study designs an MSF module to fuse and interact with features at multiple scales, as displayed in Fig. 10.

The feature extraction network is structured into three levels: low, middle, and high, with corresponding feature maps denoted as F_{L}, F_{M}, and F_{H}, respectively. To align the scale and dimensions of the low- and middle-level features with the high-level features, these features undergo a downsampling module. The downsampling module consists of a main branch and an auxiliary branch. The main branch first reduces the feature scale using a max-pooling layer, then adjusts the feature dimension with a 1×1 convolution layer.

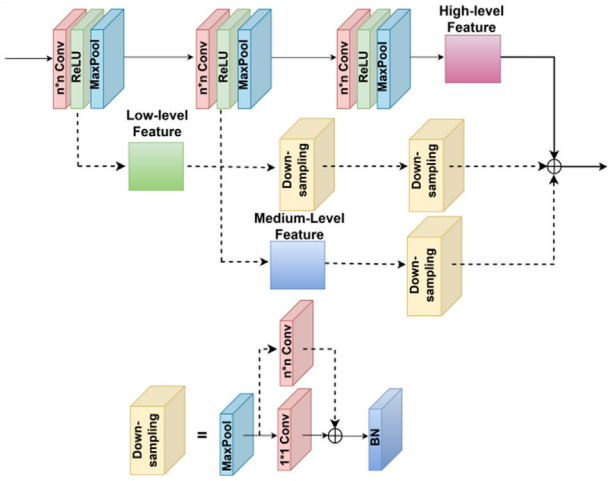

Fig. 10. Structure of multiscale feature fusion module.

$$F_{\mathrm{L}}^{\mathrm{main}} = \mathrm{Conv1} \times 1(\mathrm{MaxPool}(F_{\mathrm{L}})) \tag{7}$$

$$F_{\mathrm{M}}^{\mathrm{main}} = \mathrm{Conv1} \times 1(\mathrm{MaxPool}(F_{\mathrm{M}})) \tag{8}$$

To prevent information loss from the pooling operation, an auxiliary branch with a convolution layer is introduced in parallel to the main branch. The convolution layer in the auxiliary branch has the same kernel size and number as the pooling layer and the 1×1 convolution layer in the main branch, ensuring the dimensions of the output features correspond to those of the main branch.

$$F_{L}^{aux} = \mathrm{Convn} \times \mathrm{n}(\mathrm{MaxPool}(F_{L})) \tag{9}$$

$$F_{M}^{aux} = \mathrm{Convn} \times \mathrm{n}(\mathrm{MaxPool}(F_{M})) \tag{10}$$

Subsequently, feature maps from the main and auxiliary branches were combined and processed through a batch normalization (BN) layer to obtain the downsampled features.

$$\hat{F}_{\mathrm{L}} = \mathrm{BN}(F_{\mathrm{L}}^{\mathrm{main}} + F_{\mathrm{L}}^{\mathrm{aux}}) \tag{11}$$

$$\hat{F}_{\mathrm{M}} = \mathrm{BN}(F_{\mathrm{M}}^{\mathrm{main}} + F_{\mathrm{M}}^{\mathrm{aux}}) \tag{12}$$

The high-level feature map was then integrated element-wise with the downsampled low- and middle-level feature maps, achieving multiscale feature fusion.

$$F_{\mathrm{out}} = F_{\mathrm{H}} + \hat{F}_{\mathrm{M}} + \hat{F}_{\mathrm{L}} \tag{13}$$

This integration of multilevel feature information within the MSF module enhances the diversity and accuracy of feature extraction. Lower-layer features capture intricate details, whereas higher-layer features discern overarching trends. The synergistic combination enables the model to more effectively identify capacitor aging states, which significantly strengthens the robustness and accuracy of the model through multiscale feature fusion.

3 Simulation case verification

3.1 Dataset construction

To detect the aging state of MMC submodule capacitors, a dataset was created based on the switching states of the submodule's IGBT switches under various aging conditions. The switching state of a submodule indicates whether its IGBT switches are in the ON or OFF position, determining if the capacitor is inserted into or bypassed from the circuit. This dataset originates from MATLAB/Simulink simulations, with parameters detailed in Table 1. It comprises 7,200 data samples, including 1,200 normal samples for submodule 1 capacitors and 1,200 samples for capacitor values reduced by 1 %, 2 %, 3 %, 4 %, and 5 % each. Each sample encompasses 0.025 s of switching state data for the submodule.

3.2 Experimental Environment

This experiment was conducted on an Ubuntu 20.04 operating system, using Python version 3.8.0 and CUDA version 11.4. Training and testing were performed using the PyTorch 1.8 deep learning framework, accelerated by two NVIDIA GeForce RTX 3090-24G GPUs. The model was initially fine-tuned with pre-trained weights from the ImageNet dataset. Training spanned 100 epochs with a batch size of 8 during the transfer and frozen training phases to ensure efficiency. An initial learning rate of 0.001 was set, and the Adam optimizer was utilized to refine the training parameters.

3.3 Evaluation metrics

This study employed Top-1 Accuracy and Macro-F_1 score as quantitative metrics to evaluate classification performance. Top-1 Accuracy measures the proportion of instances where the model's predicted class exactly matches the true class, as defined in Eq. (14),

$$Top-1Accuracy = \frac{1}{N}\sum_{i=1}^{N} 1(\hat{y}_i = y_i) \tag{14}$$

where N denotes the total number of samples, $\hat{y}_i$ denotes the predicted class for the i-th sample, y_i denotes the true class for the i-th sample, and 1(ṡ) represents the indicator function (1 if the condition is true; 0, otherwise).

The F_1 score, a statistical measure for binary classification accuracy, represents the harmonic mean of precision and recall, thereby assessing the model performance as detailed in Eq. (15).

$$\mathrm{F_1} = \frac{2 \times P_{\mathrm{precision}} \times R_{\mathrm{Recall}}}{P_{\mathrm{precision}} + R_{\mathrm{Recall}}} \times 100\% \tag{15}$$

Precision represents the repeated accuracy of the model, and Recall reflects the ability of the model to capture relevant instances. The F_1 Score ranges from 0 to 1, with higher values indicating superior model performance.

Macro-F1 score is the average of the F_1 scores of all classes, reflecting the overall classification performance across multiple classes, formulated as

$$\mathrm{Macro-F_1} = \frac{1}{K} \times \sum_{i=1}^{K} F_{1i} \tag{16}$$

where K represents the number of classes. A higher Macro-F1 score signifies improved performance in multiclass classification.

Table 2
Ablation study.

Models	normal100 (F_1%)	normal99 (F_1%)	normal98 (F_1%)	normal97 (F_1%)	normal96 (F_1%)	aging95 (F_1%)	Macro-F1 (%)	Total (Top-1 %)
CSPResNeXt50 (baseline)	91.88	90.38	91.96	92.57	93.26	94.03	92.35	92.36
Deepstem	93.49	92.31	93.28	94.92	94.99	95.84	94.14	93.54
CEA	91.14	90.72	93.35	94.01	94.20	96.78	93.37	93.37
MSF	90.52	90.03	93.32	95.25	94.76	95.91	93.30	93.30
Deepstem-CEA	94.73	93.01	92.40	94.07	95.41	96.20	94.30	94.31
Deepstem-MSF	93.49	92.31	93.28	94.92	94.99	95.84	94.14	94.13
MSF-CEA	92.67	91.77	93.31	**96.86**	94.86	96.77	94.37	94.38
Deepstem-CEA-MSF	**95.18**	**93.40**	**94.39**	95.65	**96.34**	**97.93**	**95.32**	**95.49**

3.4 Ablation study

To assess the effectiveness of each module's enhancements, an ablation study was conducted. The contributions of the Deep Stem, ECA, and MSF modules to model performance were evaluated individually, and accuracy was compared using the test set. The results are presented in Table 2.

The following conclusions can be drawn from Table 2:

1) Deep Stem Module: The introduction of the Deep Stem module led to a significant increase in TOP-1 accuracy to 93.54 %, and the macro average F1 score reached 94.14 %. Compared to the baseline CSPResNeXt50 model, accuracy improved by 1.18 %, and the F1 score increased by 1.79 %. This indicates that the Deep Stem module effectively enhances feature extraction diversity and precision by gradually expanding the receptive field and smoothly integrating contextual information.
2) ECA Module: With the introduction of the ECA module, the TOP-1 accuracy reached 93.37 %, and the macro-averaged F_1 score was also 93.37 %, indicating an accuracy improvement of 1.01 % and an F_1 score increase of 1.02 %. The ECA module dynamically modulates channel weights via adaptive 1D convolutions, enabling the network to more effectively detect subtle variations and critical features in capacitor aging, thereby enhancing the recognition capabilities of the model.
3) MSF Module: Integrating the MSF module resulted in TOP-1 accuracy and macro average F_1 scores reaching 93.30 %, with each metric increasing by 0.94 %. The MSF module augments the ability of the model to capture short-term complex changes and long-term trends in capacitor aging by merging features across multiple scales.
4) Combined Modules: Employing the Deep Stem and ECA modules together achieved TOP-1 accuracy and macro average F_1 scores of 94.31 % and 94.30 %, respectively. Combining the Deep Stem and MSF modules yielded TOP-1 accuracy and macro average F_1 scores of 94.14 %. The integration of the ECA and MSF modules resulted in TOP-1 accuracy and macro average F_1 scores of 94.38 % and 94.37 %, respectively. When all three modules were incorporated, performance peaked with a TOP-1 accuracy of 95.49 % and a macro average F_1 score of 95.32 %, significantly surpassing the baseline model. These results further confirm the synergistic effects of the modules in enhancing overall model performance.

In summary, the ablation study clearly demonstrates the significant role of the Deep Stem, ECA, and MSF modules in improving the ability of the model to recognize capacitor aging states. The integration of these modules yields superior performance enhancements, confirming the effectiveness and practicality of the improved components.

3.5 Comparative validation

To validate the proposed approach, we benchmarked it against traditional deep learning models, including DenseNet [21], EfficientNet_v2 [22], MobileNet_v3 [23], and the original CSPResNeXt-50 network. The results are outlined in Table 3.

Our method attained a TOP-1 accuracy of 95.32 % on the capacitor aging test set, markedly outperforming other conventional deep learning architectures. These findings demonstrate that the enhancements introduced in this study significantly improve the model's classification accuracy. Specifically, relative to the original CSPResNeXt-50

Table 3
Comparative training results for multiple classification models.

Models	normal100 (F_1%)	normal99 (F_1%)	normal98 (F_1%)	normal97 (F_1%)	normal96 (F_1%)	aging95 (F_1%)	Macro-F_1(%)	Total (Top-1 %)
CSPdarknet50	86.08	84.92	89.58	90.93	90.53	92.45	89.08	89.10
CSPResNet50	85.38	84.17	87.31	89.74	89.12	90.15	87.65	87.67
CSPResNeXt50	91.88	90.38	91.96	92.57	93.26	94.03	92.35	92.36
CapAgingNet	**95.18**	**93.40**	**94.39**	**95.65**	**96.34**	**97.93**	**95.32**	**95.49**
Resnext50	87.78	84.05	86.90	89.70	90.02	91.95	89.40	88.44
Res2net50	87.72	85.28	90.30	91.40	92.77	94.12	90.27	90.31
Densenet121	74.14	66.89	80.66	82.76	83.49	87.53	79.25	79.31
Efficientnetv2_b3	55.42	43.55	42.47	50.67	44.30	60.18	49.43	48.78
Mobilenet v3 small	70.99	64.96	63.12	70.75	71.91	74.12	69.31	69.48
Shufflenet_v2	71.80	63.92	82.04	88.49	86.86	92.67	80.96	74.06
SEResNeXt50	85.98	83.59	88.03	91.83	90.31	91.46	88.53	88.54

network, our approach increased the TOP-1 accuracy on the test set by 3.17 percentage points and the macro average F_1 score by 2.97 percentage points. As illustrated in Table 3, the CapAgingNet model excelled in categorizing all aging levels. For example, the F_1 score for the aging95 category achieved 97.93 %, considerably higher than that of competing models.

Moreover, analysis of accuracy and loss functions before and after the enhancements (Fig. 11) indicates that the improved network achieves higher accuracy and lower loss values during training. This suggests that the enhanced network converges more rapidly and possesses greater generalization capabilities. Specifically, in the early training stages, the improved network rapidly achieves higher accuracy and remains stable in later stages. The results further substantiate the benefits of the Deep Stem, ECA, and MSF modules in feature extraction and integration.

Comparing the confusion matrices before and after enhancements (Fig. 12) reveals a substantial reduction in misclassifications across all categories. Particularly, the classification accuracy is significantly improved for the normal97 and aging95 categories. Therefore, the enhanced model achieves greater accuracy and stability in differentiating various stages of capacitor aging, thereby more effectively identifying capacitor aging states.

In summary, the integrated Deep Stem, ECA, and MSF modules showcase superior performance in detecting capacitor aging states, markedly surpassing traditional deep learning methods and the original CSPResNeXt-50 network. This affirms the effectiveness of the proposed method and its potential for practical applications.

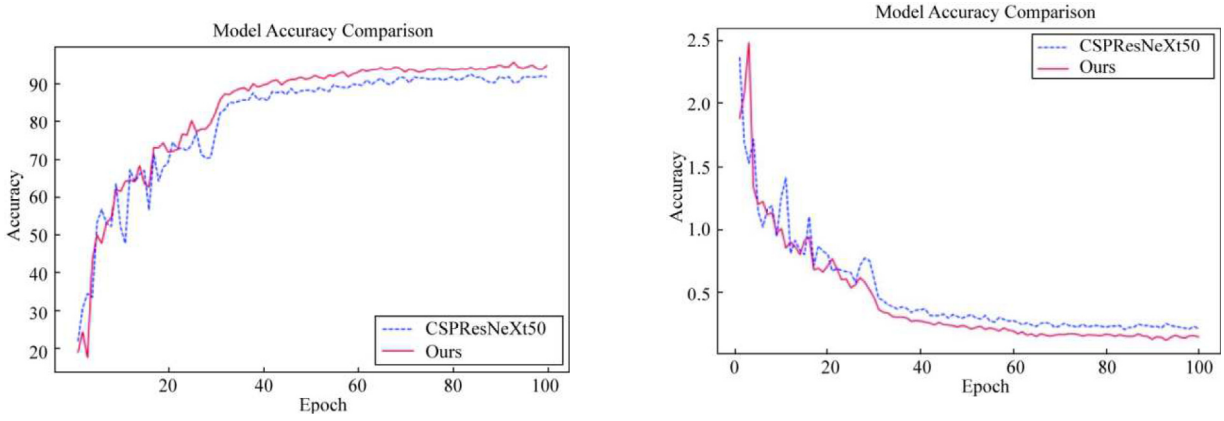

(a) Model accuracy function before and after improvement

(b) Model loss function before and after improvement

Fig. 11. Comparison of model accuracy and loss function before and after improvement.

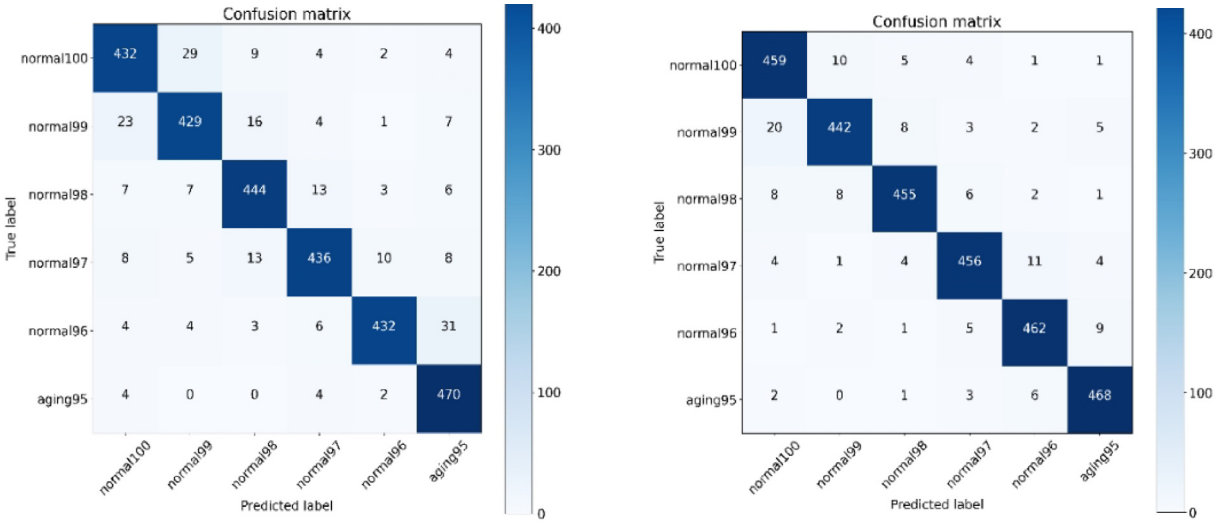

(a) Model confusion matrix before improvement

(b) Model confusion matrix after improvement

Fig. 12. Model confusion matrix before and after improvement.

4 Conclusions

This study addresses the issue of submodule capacitor aging in MMC by introducing an online capacitor aging evaluation method based on capacitor switching state information. The main conclusions are as follows:

1) Analysis of MMC Operation and Capacitor Aging Mechanism: The study begins with a comprehensive analysis of MMC operating principles and the aging mechanisms of metallized film capacitors. It examines how capacitor aging affects submodule switching states and identifies the key factors influencing system performance due to capacitor aging.
2) Design and Integration of Improved Modules: To address the shortcomings in the feature extraction of the traditional models, three improved modules were designed and introduced: the Deep Stem module, ECA module, and the MSF module. The Deep Stem module incrementally enlarges the receptive field, enhancing the diversity and precision of feature extraction while addressing deficiencies in low-level feature representation. The ECA module modulates channel weights via adaptive dynamic 1D convolution, thereby amplifying the representation of salient features and enhancing feature capture across the channel dimension. The MSF module integrates multilevel features, boosting the accuracy and robustness of feature extraction and mitigating the loss of multiscale features. These optimized modules were incorporated into the CSPResNeXt-50 architecture, resulting in the newly developed CapAgingNet model.
3) Experimental Results: The experimental findings indicate that CapAgingNet delivers outstanding performance in capacitor aging detection, achieving substantial gains in accuracy and macro-average F_1 score. It effectively captures subtle variations in capacitor switching states, enabling precise determination of their aging conditions. Ablation studies and comparative analyses further validate the efficacy of each module and the considerable enhancements they offer. CapAgingNet surpasses conventional deep learning approaches and the original CSPResNeXt-50 network in classification accuracy and model stability.
4) Future Research Directions: This research concentrates on evaluating the aging of individual submodule capacitors. Future research could investigate the interplay of aging among multiple submodule capacitors. The aging states of several modules may involve intricate interactions and propagation mechanisms, necessitating further exploration and modeling. Furthermore, incorporating more real-world operational data and scenarios can validate and optimize the performance and stability of the CapAgingNet model to overcome the challenges of practical applications in complex power electronic systems. Future research will further develop online capacitor aging assessment technologies within systems like MMC, offering theoretical and practical support to improve system reliability and operational efficiency.

Declaration of competing interest

DENG Youhan and YAO Weiwei are currently employed by Science and Technology Research Institute, China Three Gorges Corporation.

Acknowledgements

This work was supported by China Yangtze Power Co., Ltd. (No. ZSF2502001).

References

[1] M. Hagiwara, H. Akagi, Control and experiment of pulsewidth-modulated modular multilevel converters, IEEE Trans. Power Electron. 24 (7) (2009) 1737–1746.
[2] D.G. Xu, B.B. Li, S.Z. Zhou, Overview of the modular multilevel converter based high voltage motor drive, Trans. China Electrotechn. Soc. 32 (20) (2017) 104–116.
[3] M. Xiao, Y.Y. Chen, Y.S. Zhao, et al., Research progress in improving insulation properties of HVDC metalized film capacitor, High Volt. Eng. 50 (6) (2024) 2319–2331.
[4] W.Y. Zhang, L. Qi, X.Y. Zhang, et al., Reliability evaluation method for VSC-HVDC valve submodules considering the correlation between the degradation process of metallized polypropylene film capacitors and IGBT modules, Trans. China Electrotechn. Soc. 39 (14) (2024) 4508–4518.
[5] P.Y. Huang, H. Nagasaki, T. Shimizu, Capacitor characteristics measurement setup by using B–H analyzer in power converters, IEEE Trans. Ind. Appl. 54 (2) (2017) 1602–1613.
[6] Y.J. Jo, T.H. Nguyen, D.C. Lee, Capacitance estimation of the submodule capacitors in modular multilevel converters for HVDC applications, J. Power Electron. 16 (5) (2016) 1752–1762.
[7] D. Ronanki, S.S. Williamson, Failure prediction of submodule capacitors in modular multilevel converter by monitoring the intrinsic capacitor voltage fluctuations, IEEE Trans. Ind. Electron. 67 (4) (2020) 2585–2594.
[8] H.Y. Wang, H. Wang, Z.X. Wang, et al., Condition monitoring for submodule capacitors in modular multilevel converters, IEEE Trans. Power Electron. 34 (11) (2019) 10403–10407.
[9] K. Wang, L. Jin, G.D. Li, et al., Online capacitance estimation of submodule capacitors for modular multilevel converter with nearest level modulation, IEEE Trans. Power Electron. 35 (7) (2020) 6678–6681.
[10] J.V.M. Farias, L.A. Grégoire, A.F. Cupertino, et al., A sliding-mode observer for MMC-HVDC systems: fault-tolerant scheme with reduced number of sensors, IEEE Trans. Power Delivery 38 (2) (2023) 867–876.
[11] F.J. Deng, Q.S. Wang, D. Liu, et al., Reference submodule based capacitor monitoring strategy for modular multilevel converters, IEEE Trans. Power Electron. 34 (5) (2019) 4711–4721.
[12] Q.X. Pu, L. Qin, Q. Wang, et al., (2022) On-line monitoring and balancing strategy for capacitor aging in modular multilevel converter, Electr. Measur. Instrument. 59 (7) (2022) 193–200.
[13] H.J. Xia, M.Y. Chen, W. Lai, et al., Failure detection method for metalized polypropylene film capacitor in modular multilevel converter based on band energy, Proc. CSEE 41 (22) (2021) 7782–7793.

[14] Y.J. Wu, J.B. Zhang, W. Lai, et al., Residual life assessment method based on on-line condition monitoring of metallised film capacitors, Trans. China Electrotechn. Soc. (2024), https://doi.org/10.19595/j.cnki.1000-6753.tces.231752.
[15] H.J. Xia, Y. Zhang, M.Y. Chen, et al., Capacitor parameter estimation based on wavelet transform and convolution neural network, IEEE Trans. Power Electron. 39 (11) (2024) 14888–14897.
[16] L.Z. Zheng, L.Y. Zhu, S.C. Ji, et al., Study on online acquisition method of multi-frequency dielectric loss tangent of metallized film capacitor for MMC-HVDC, Power Capacitor React. Power Compensat. 41 (4) (2020) 63–68.
[17] Z.Y. Li, J.R. Wang, Z. Xu, et al., Self-healing characteristics and life prediction of metallized film capacitor under DC voltage, High Voltage Eng. 49 (7) (2023) 2929–2937.
[18] H. Wang, F. Blaabjerg, Reliability of capacitors for DC-link applications in power electronic converters: an overview, IEEE Trans. Ind. Appl. 50 (5) (2014) 3569–3578.
[19] C.Y. Wang, H.Y. Mark Liao, Y.H. Wu, et al., CSPNet: a new backbone that can enhance learning capability of CNN, 2020 IEEE/CVF Conference on Computer Vision and Pattern Recognition Workshops (CVPRW), 2020.
[20] Q.L. Wang, B.G. Wu, P.F. Zhu, et al., ECA-net: efficient channel attention for deep convolutional neural networks, in: Proceedings of 2020 IEEE/CVF Conference on Computer Vision and Pattern Recognition (CVPR), IEEE, USA, 2020, pp. 11531–11539.
[21] G. Huang, Z. Liu, L.V. Maaten, et al., Densely Connected Convolutional Networks, 2018, Available via DIALOG, https://arxiv.org/pdf/1608.06993.pdf, Accessed 15 MAY 2024.
[22] M. Tan, Q.V. Le, EfficientNetV2: Smaller Models and Faster Training, 2021, Available via DIALOG, https://arxiv.org/abs/2104.00298.pdf, Accessed 15 MAY 2024.
[23] A. Howard, M. Sandler, B. Chen, et al., Searching for MobileNetV3, in: Proceedings of 2019 IEEE/CVF International Conference on Computer Vision (ICCV), IEEE, Seoul, Korea, 2019, pp. 1314–1324.

Deng Xinlan received a bachelor's degree at Wuhan University, Wuhan, in 2022. She is working towards a master's degree at Wuhan University, Wuhan. Her research interests include the application of artificial intelligence technology in the field of power electronics.

Deng Youhan received his Ph.D. degree at Wuhan University in 2014. He is currently a Senior Engineer in China Three Gorges Corporation. His main research direction is power system operation and control.

Qin Liang received a bachelor's degree at Wuhan University, Wuhan, in 2003, and a Ph. D. degree at Wuhan University, Wuhan, in 2008. He is currently an associate professor in the School of Electrical and Automation at Wuhan University and a Ph. D., Deputy Director of the Institute of Power Electronics and Electrical Machines and Deputy Director of Hubei Key Laboratory of Integrated Energy Power Equipment and System Safety at Wuhan University. His research interests include analysis and control of power electronic power systems (flexible DC systems, renewable energy generation), and artificial intelligence analysis and control based on big data mining.

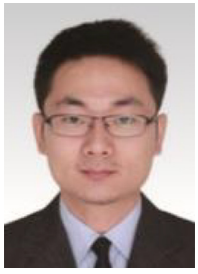

Yao Weiwei received his Ph.D. degree at Wuhan University in 2021. He is currently a Senior Engineer in China Three Gorges Corporation. His main research direction is power system operation and control.

He Min received a bachelor's degree at Wuhan Textile University, Wuhan, in 2018. He is working towards a Ph.D. degree at Wuhan University, Wuhan. His research interests include the application of artificial intelligence technology in power systems.

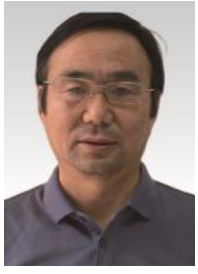

Kaipei Liu received his bachelor's, master's, and Ph.D. degrees in automation, power plant engineering, and computer application technology from Wuhan University in 1984, 1987, and 2001 respectively, Wuhan. He is currently a Professor at the School of Electrical Engineering, at Wuhan University. He has authored over 200 publications in research journals with funding from NDRC, MOST, NSFC, and corporate sponsors. His research interests include DC transmission and distribution, renewable energy and smart grid, power quality, and data analysis.